Eur. Phys. J. D **21**, 285–291 (2002)
DOI: 10.1140/epjd/e2002-00206-0

THE EUROPEAN PHYSICAL JOURNAL D

Photo double ionization of He: C3-like wave function for the two electron continuum

S. Otranto[1,2,a] and C.R. Garibotti[1]

[1] CONICET and Centro Atómico Bariloche, 8400 S. C. de Bariloche, Argentina
[2] Departamento de Física, Universidad Nacional del Sur, 8000 Bahía Blanca, Argentina

Received 19 June 2002 / Received in final form 15 August 2002
Published online 8 October 2002 –

Abstract. We evaluate the triply differential cross-section (TDCS) for photo double ionization of helium. We use a C3 final continuum wave function with an interelectronic effective coordinate to express the nuclear screening. Comparison with the standard C3 model shows that the TDCS is enhanced in the threshold region by effect of the reduced interelectronic repulsion introduced by the present model. A more accurate description of the intermediate energy region is also obtained. Comparison with recent experimental data shows a good overall agreement of the angular distributions. The theoretical PDI total cross-section shows a relevant improvement in the intermediate energy region relative to the C3 model, which converges to data for photon energies larger than 1 keV.

PACS. 32.80.Fb Photoionization of atoms and ions

1 Introduction

In the last few years, many efforts have been displayed towards the experimental and theoretical understanding of the ejection of two electrons from an atom due to single photon impact. Although theoretical work begins about 40 years ago [1], measurements of the triply differential cross-section (TDCS) for this process were not available until the last decade. A description of recent experimental and theoretical work can be found in two recent reviews [2,3].

Since photons do not distort the initial states as charged particles do, the initial state to be considered is the unperturbed ground state when He atoms are used. The final system is defined by a pure three body Coulomb state in the continuum. Initial states of different accuracy have been obtained using variational methods since the 1930s. However, the situation complicates for the description of the three body continuum. A first approximation to the final state can be obtained by neglecting the $e-e$ interaction and the non-orthogonal kinetic energy. This leads to the C2 model which proposes as solution a product of two independent Coulomb waves times plane waves. Byron and Joachain, used this final state and showed that this model gives reasonable values of the total cross-section for photo double ionization (PDI) [4]. Shakeshaft and collaborators [5,6] proposed the 2SC method, where the final state $\Psi_{\rm f}$ is given as in the C2 function, but with screened momentum-dependent effective nuclear charge, as first proposed by Rudge and Seaton [7]. This method proved to give accurate results in magnitude and shape for the equal energy sharing of the exceeding energy by the emitted electrons [8].

The interelectronic potential is entirely considered by the C3 approximation firstly introduced by Garibotti and Miraglia [9] in ion–atom collisions and later applied to electron–atom collisions by Brauner *et al.* [10]. The C3 wave function mainly consists in the product of three Coulomb waves, each one representing the interaction between a pair of particles. Maulbetsch and Briggs, applied the C3 model to calculate TDCSs for PDI of He [11], comparing its results with the C2 final state. The C2 approximation erroneously predicts a finite TDCS for $\mathbf{k}_1 = \mathbf{k}_2$ (being $\mathbf{k}_{1,2}$ the momenta of the emitted electrons). Due to the repulsive character of the interelectronic interaction, a zero TDCS should be expected in that limit [11]. The C3 wave function besides satisfying the selection rules, gives results which are in excellent agreement in shape with the experimental data for both equal and unequal energy sharing regime. This theory, however gives very low absolute probabilities at low energies above the threshold, and predicts absolute values of the TDCS, which decrease exponentially in the threshold region. This is mainly due to the normalization factor associated with the $e-e$ interaction [8], which predicts an exponential decay as the energy decreases, instead of the power law dependence resulting from Wannier theories. The C3 model accounts for the repulsion correlation but misses the kinetic correlation given by the non-orthogonal kinetic energy [12]. The kinetic correlation could be partially considered by

[a] e-mail: sotranto@uns.edu.ar

introducing effective Sommerfeld parameters, depending on the coordinates and momentums [13–16]. However, this methodology applied to PDI proved to be not as efficient as in electron–atom collisions, where an improvement of the near threshold region has been achieved.

In the last few years, other approaches have succeeded in obtaining accurate triply differential cross-sections (TDCSs). The convergent close-coupling approach [17] and the time-dependent close-coupling method [18] have proved to give reliable predictions of PDI processes in magnitude and angular shape also. Furthermore, their theoretical predictions in the velocity, length and acceleration gauges, get coincident in a wide range of photon energies as the number of parameters of a Hylleras-type initial wave function is increased. Another successful calculation has been recently presented by Malegat *et al.* [19] using the ab initio hyperespherical R-matrix method with semiclassical outgoing waves. They find excellent agreement with the experimental data and good agreement between gauges.

However, an analytical final state wave function that assures such an accuracy is not still available and is field of continuous interest and research. The TDCS for PDI is mainly determined by the final state wave function when the three Coulomb-interacting particles are near (*i.e.* $r_1, r_2 < 20$ a.u.) [15]. Usual approximated solutions have been generated by continuation to short distances of the correct asymptotic condition in the Ω_0 region of the configuration space, in which all three interparticle distances are large. This methodology does not assure that the inner region is appropriately described though. Similar comments can be done for the final state wave function recently introduced by Miraglia *et al.* [20] in terms of the natural base. This base, presents the advantage that the non-orthogonal kinetic energy usually neglected, could then be partially incorporated through an expansion in terms of Kummer functions.

Ward and Macek [21], have obtained approximated wave functions to represent the two electron continuum. They define an average fixed interelectronic distance, which, properly chosen, compensates the exponential decay of the C3 model near threshold. This average distance only depends in the total energy of electrons. However, these functions have the drawback that violate the Redmond asymptotic condition in the Ω_0 region.

In this work, we propose as final state wave function a modified version of the C3 model, following the aim of Ward and Macek. We perform a dilatation of the interelectronic coordinate, by multiplying it by a energy dependent real coefficient. Here, the interelectronic coordinate is not fixed, and this assures validity of the Redmond asymptotic conditions.

In Section 2, the theory is presented. In Section 3 results are shown. The differential cross-sections for 6 eV and 20 eV exceeding energy and the PDI total cross-section are calculated using the C3 wave and the present model. The results are compared with available experimental data. In Section 4, some conclusions are drawn. Atomic units are used unless otherwise explicitly stated.

2 Theory

The triply differential cross-section (TDCS) for absorption of a photon of energy E_ω and emission of two electrons with momenta $\mathbf{k}_1, \mathbf{k}_2$ is given by:

$$\frac{\mathrm{d}\sigma}{\mathrm{d}\Omega_1 \mathrm{d}\Omega_2 \mathrm{d}E_1} = 4\pi^2 \alpha k_1 k_2 C^{(G)} \left| T_{\mathrm{fi}}^{(G)} \right|^2$$

where α is the fine-structure constant. The energies of the electrons are $E_1 = k_1^2/2$ and $E_2 = k_2^2/2$, and $E_\mathrm{f} = E_1 + E_2$ the total final energy. The $T_{\mathrm{fi}}^{(\mathrm{G})}$ transition amplitude is given by

$$T_{\mathrm{fi}}^{(\mathrm{G})} = \left\langle \Psi_\mathrm{f} | \widehat{\varepsilon} \cdot \mathbf{O}^{(\mathrm{G})} | \Psi_\mathrm{i} \right\rangle . \tag{1}$$

Here, the operator $\mathbf{O}^{(\mathrm{G})}$ represents the matter-radiation interaction in the dipole approximation. It could be expressed in three different gauges: $\mathbf{O}^{(\mathrm{V})} = \nabla_1 + \nabla_2$, $\mathbf{O}^{(\mathrm{L})} = \mathbf{r}_1 + \mathbf{r}_2$ and $\mathbf{O}^{(\mathrm{A})} = Z_\mathrm{T} \left(\mathbf{r}_1 / r_1^3 + \mathbf{r}_2 / r_2^3 \right)$, where V, L, A denote respectively velocity, length and acceleration gauges. The coefficients $C^{(\mathrm{G})}$ are given by: $C^{(\mathrm{V})} = E_\gamma^{-1}, C^{(\mathrm{L})} = E_\gamma, C^{(\mathrm{A})} = E_\gamma^{-3}$.

The Ψ_f wave function represents the final state, where the two electrons are in the continuum sharing the exceeding energy of the annihilated photon, and the Ψ_i wave function, represents the He ground state. We consider a linearly polarized photon incident in the direction of the axis x with polarization vector $\widehat{\varepsilon}$ in the direction of the z-axis. One of the electrons is emitted in the plane orthogonal to the x-axis with angle θ_2 relative to z. The direction of the other is determined by the angles ϕ_1, relative to the yz-plane, and θ_1 relative to $\widehat{\varepsilon}$.

The continuum of two electrons, has been usually represented by a C3 model [9,10],

$$\begin{aligned} \Psi_{\mathrm{C3}}(\mathbf{k}_1, \mathbf{k}_2, \mathbf{r}_1, \mathbf{r}_2) = N_\mathrm{f}\, \mathrm{e}^{\mathrm{i}\mathbf{k}_1 \cdot \mathbf{r}_1 + \mathrm{i}\mathbf{k}_2 \cdot \mathbf{r}_2}\, {}_1F_1[\mathrm{i}a_1, 1, x_1] \\ \times_1 F_1[\mathrm{i}a_2, 1, x_2]\, {}_1F_1[\mathrm{i}a_3, 1, x_3]. \end{aligned} \tag{2}$$

The coefficients $a_i = Z_i \mu_i / k_i$ are the Sommerfeld parameters, $x_i = -\mathrm{i}k_i \xi_i$ and $\xi_i = r_i + \widehat{\mathbf{k}}_i \cdot \mathbf{r}_i$, $i = 1, 2, 3$ are generalized parabolic coordinates corresponding to each pair of particles. Here, Z_i, μ_i and k_i indicate charges, reduced masses and momentum of each electron relative to nucleus and between the electrons, respectively. The normalization factor is fixed by the Redmond condition and is given by:

$$N_\mathrm{f} = \frac{1}{(2\pi)^3} \prod_{j=1}^{3} \mathrm{e}^{-a_j \frac{\pi}{2}} \Gamma(1 - \mathrm{i}a_j). \tag{3}$$

The term with $j = 3$ corresponds to the $e-e$ repulsion and produces a exponential decay of the TDCS at small relative energies. Brauner *et al.* have shown that with the factor N_f the C3 wave function is normalized to a six dimensional delta function [22],

$$\int \Psi_{\mathrm{C3}}^*(\mathbf{k}_1', \mathbf{k}_2', \mathbf{r}_1, \mathbf{r}_2) \Psi_{\mathrm{C3}}(\mathbf{k}_1, \mathbf{k}_2, \mathbf{r}_1, \mathbf{r}_2) \mathrm{d}\mathbf{r}_1 \mathrm{d}\mathbf{r}_2 = \delta(\mathbf{k}_1' - \mathbf{k}_1) \delta(\mathbf{k}_2' - \mathbf{k}_2).$$

This equation must be interpreted in the distribution sense, and defined with a support weight function. Equation (3) indicates that the norm of the hypergeometric functions in the C3 wave increases in the limit $E_\mathrm{f} \to 0$, to compensate the exponential decay of the normalization factor at this energy limit. Otherwise, the transition amplitude in equation (1) is mathematically a scalar product of a C3 wave function with the function resulting from the interaction and the initial state. The value of this matrix element depends of the superposition of these functions in the configuration space. It seems clear that the increase of the norm of the hypergeometric functions is not enough to compensate the normalization factor decrement as energy approaches the threshold.

To correct this failure of the C3 model, Ward and Macek [21] replace the interelectronic distance in the third hypergeometric of the C3 function by a fixed average distance (x_3^{ave}). This x_3^{ave} only depends in the total energy of electrons and its functional form is determined by requiring that the doubly differential cross-section satisfies the Wannier limit at the threshold. However, these functions have the drawback that are obtained sacrificing the Redmond asymptotic condition in the Ω_0 region,where the particles are far away from each other. Large distance behavior of the wave function would not have much relevance for PDI but it is important if one desires to use this wave function in electron–atom collisions also.

Here we propose an alternative procedure by representing the continuum of two electrons with the following wave function,

$$\Psi_{\mathrm{SC3}}(\mathbf{k}_1,\mathbf{k}_2,\mathbf{r}_1,\mathbf{r}_2) = N_\mathrm{f}\,\mathrm{e}^{\mathrm{i}\mathbf{k}_1\cdot\mathbf{r}_1+\mathrm{i}\mathbf{k}_2\cdot\mathbf{r}_2}\,{}_1F_1[\mathrm{i}a_1,1,x_1] \times{}_1F_1[\mathrm{i}a_2,1,x_2]\,{}_1F_1[\mathrm{i}a_3,1,\beta\,x_3]. \quad (4)$$

The normalization constant N_f is obtained by requiring the wave function to have outgoing unitary flux. The asymptotic behavior of the wave function in the Ω_0 region is given by

$$\Psi_{\mathrm{SC3}} \xrightarrow[x_{1,2,3}\to\infty]{} N_\mathrm{f}\,\mathrm{e}^{\mathrm{i}\mathbf{k}_1\cdot\mathbf{r}_1+\mathrm{i}\mathbf{k}_2\cdot\mathbf{r}_2} \times\prod_{j=1}^{3}\frac{\mathrm{e}^{\frac{\pi}{2}a_j}}{\Gamma(1-\mathrm{i}a_j)}\mathrm{e}^{-\mathrm{i}a_3\log(\beta)}\mathrm{e}^{-\mathrm{i}a_j\log(x_j)}.$$

It could be seen that the Redmond asymptotic conditions are fulfilled, and that the β parameter appears asymptotically only through a phase factor. Therefore the normalization remains as that of the C3 function.

We now analyze the Wannier region with this final wave and a simple Slater initial state $\Psi_\mathrm{i} = N_\mathrm{i}\mathrm{e}^{-Z_s(r_1+r_2)}$ and in the velocity gauge. We assume that the electrons leave the nuclear charge "almost" collinear and with equal energy. Using integral representations of the Kummer hypergeometric functions and neglecting terms of order k^2 the transition amplitude gives:

$$\begin{aligned}T_{\mathrm{fi}}^{\mathrm{V}} = &-\frac{1}{Z_s^6}N_\mathrm{i}N_\mathrm{f}\widehat{\varepsilon}\cdot\mathcal{B}\int_0^1\mathrm{d}t \times\int_0^1\mathrm{d}u\int_0^1\mathrm{d}v\,t^{\mathrm{i}a_3^*-1}(1-t)^{-\mathrm{i}a_3^*}u^{\mathrm{i}a_1^*-1}(1-u)^{-\mathrm{i}a_1^*} \times v^{\mathrm{i}a_2^*-1}(1-v)^{-\mathrm{i}a_2^*}\left[\frac{\mathrm{i}64\pi^2(Z_s-\mathrm{i}k2\beta t-\mathrm{i}k2v)k\widehat{\mathbf{k}}_1}{Z_s-16\mathrm{i}k\beta t-8\mathrm{i}k(v+u)}\right.\\ &\left.+\frac{\mathrm{i}64\pi^2(Z_s-\mathrm{i}k2\beta t-\mathrm{i}k2u)k\widehat{\mathbf{k}}_2}{Z_s-16\mathrm{i}k\beta t-8\mathrm{i}k(v+u)}\right]\end{aligned}$$

where $\mathcal{B}$ is given by

$$\mathcal{B} = \prod_{j=1}^{3}\frac{1}{\Gamma(\mathrm{i}a_j^*)\Gamma(1-\mathrm{i}a_j^*)}\,.$$

As $0 < u,\ v < 1$ and $k \to 0$ we neglect terms of order ku and kv, and integrating over the parameters t, u, v we obtain,

$$T_{\mathrm{fi}}^{\mathrm{V}} = -\frac{\mathrm{i}8\pi^2k}{Z_s^6}N_\mathrm{i}N_\mathrm{f}\left[1+7\left(1-\frac{16\mathrm{i}k\beta}{Z_s}\right)^{\frac{\mathrm{i}}{2k}}\right] \times\widehat{\varepsilon}\cdot\left(\widehat{\mathbf{k}}_1+\widehat{\mathbf{k}}_2\right). \quad (5)$$

The first term, does not contribute near threshold due to the exponential decay of the normalization constant N_f and can be neglected. The normalization constant $|N_\mathrm{f}|^2$ is given in this limit by [22],

$$|N_\mathrm{f}|^2 = (4\pi)^2\frac{\pi}{k^2}\frac{\mathrm{e}^{-\frac{\pi}{\sqrt{E_\mathrm{f}}}\left(1+\frac{(\pi-\theta_{12})^2}{8}\right)}}{\sqrt{E_\mathrm{f}}}\,.$$

The Gaussian factor is in concordance with the results of the second order Wannier theory, but the remaining exponential factor produces the fall of the theoretical TDCS for small k. Then finally we obtain the following limit expression for the TDCS

$$\frac{\mathrm{d}\sigma}{\mathrm{d}\Omega_1\mathrm{d}\Omega_2\mathrm{d}E_1} = \frac{3136N_i^2\alpha\pi^3}{E_\gamma\,Z_s^{12}}\sqrt{E_\mathrm{f}}\mathrm{e}^{\frac{1}{\sqrt{E_\mathrm{f}}}\left(\arctan\left[\frac{16\sqrt{E_\mathrm{f}}\beta}{Z_s}\right]-\pi\right)} \times\mathrm{e}^{-\frac{\pi(\pi-\theta_{12})^2}{8\sqrt{E_\mathrm{f}}}}(\cos\theta_1+\cos\theta_2)^2.$$

Note that in the threshold the equal sharing emission is dominant and $E_\mathrm{f} = 2E_1$.

Now we must give an explicit expression for the β. Correlation effects are expected to be neglectfull when the exceeding energy $E_\mathrm{f} \to \infty$, and the transition amplitude is correctly given by the C2 model. Therefore is reasonable to require that $\beta \to 0$ in the high energy limit. We will assume a simple energy dependence:

$$\beta = \frac{1}{\sqrt{E_\mathrm{f}}}. \quad (6)$$

Then the TDCS reads

$$\frac{\mathrm{d}\sigma}{\mathrm{d}\Omega_1 \mathrm{d}\Omega_2 \mathrm{d}E_1} = \frac{3136 N_i^2 \alpha \pi^3}{E_\gamma\, Z_s^{12}} \sqrt{E_\mathrm{f}} \mathrm{e}^{\frac{\arctan\left[\frac{16}{Z_s}\right]-\pi}{\sqrt{E_\mathrm{f}}}} \times \mathrm{e}^{-\frac{\pi(\pi-\theta_{12})^2}{8\sqrt{E_\mathrm{f}}}} (\cos\theta_1 + \cos\theta_2)^2. \quad (7)$$

Then it can be easily seen that the introduction of the factor $\exp[\arctan(16\sqrt{E_\mathrm{f}}\beta/Z_s)/\sqrt{E_\mathrm{f}}]$ leads to an enhancement of the TDCS for $E_\mathrm{f} \to 0$ with respect to the standard C3 model. The last factor is the so-called "angular factor" and it is obtained when simple plane waves are used to represent the final state.

The ground state correlation effects are expected to be small for low energy photons and equal energy sharing emission but are more relevant for the unequal energy sharing regime. Therefore we consider one of the simplest correlated states for the ground state function of helium:

$$\Psi_{\mathrm{GS2a}} = N_\mathrm{i}(\mathrm{e}^{-c_1 r_1 - c_2 r_2} + \mathrm{e}^{-c_2 r_1 - c_1 r_2}) \times (\mathrm{e}^{-z_\mathrm{c} r_{12}} + C_0 \mathrm{e}^{-\lambda r_{12}}) \quad (8)$$

with $N_\mathrm{i} = 1.71749$, $c_1 = 1.4096$, $c_2 = 2.2058$, $C_0 = -0.6244$, $z_\mathrm{c} = 0.01$ and $\lambda = 0.244712$. This gives a bounding energy $\langle E \rangle = -2.9019$ a.u. Note that $\langle E_\mathrm{exact} \rangle = -2.903724$ a.u. The cusp condition value at the nucleus for He is given by $(\partial\Psi_i/\partial r_{1,2})_{r_{1,2}=0}/(\Psi_i)_{r_{1,2}=0} = -2$, for the exact wave function. The cusp condition value at the nucleus for the Ψ_{GS2a} wave function is $R_\mathrm{cusp} = -1.807$. This wave function is an adaptation of the Bonham and Kohl GS2 correlated state [23], where we have calculated the variational parameters to use z_c, and avoid a cut-off. This simple functional form allows for a calculation of the transition amplitude using Nordsieck-like integrals [24].

We have used the final and initial waves given by equations (4, 8) respectively to evaluate the TDCS for photo double ionization of helium as shown below. We choose β according to equation (6). This β factor, leads to an enhancement of the TDCS for $E_\mathrm{f} < 2R_\mathrm{y}$ and a diminishing TDCS for $E_\mathrm{f} > 2R_\mathrm{y}$, where R_y is the Rydberg constant. For the equal energy sharing Maulbetsch *et al.* [25] have shown that the C3 model overestimates (underestimates) the TDCS magnitude for E_f above (below) $2R_\mathrm{y}$. Kornberg and Miraglia estimate that correct magnitudes are reached with the C3 model for E_f above 1 keV [24]. In this sense our β selection tends to correct the failure of the C3 model not only in the low but also in the intermediate energy region as will be shown in the next section.

3 Results

We compare our theoretical results with the experimental data obtained by Dörner *et al.* [26] using the COLTRIMS technique [27]. With this technique one of the emitted electrons is measured in coincidence with the recoil ion and the dynamic of the three particles is given by conservation rules. To collect a sufficient number of coincidence events the detection solid angles must be large. For comparison with experiment the theoretical values must be averaged inside the detection volume determined by the energy and angular resolutions. This is a large computational task, when using the wave function in equation (4). We have performed averages of TDCSs up to 15 points (fifteen different angular configurations inside the detection volume) finding out that an angular five-point average is enough to obtain a stable description of the main features. Therefore, we average our TDCSs over a five point angular configuration (θ_1^i, ϕ_1^i) $i = 1, ..., 5$ within the angular resolution, at the mean detection energy. The well known selection rules [28], predict zeros for the TDCS for certain angular configurations, at equal electron energy sharing. These zeros become smoothed by the superposition of angular configurations giving well established minimums in the distributions. When $\theta_1 = 40°$ and $\varphi_1 = \varphi_2 = 0$ the selection rules predict zeros for the TDCS at $\theta_2 = 40°, 140°$ and 220° [28]. Equivalent zeros occur for other values of θ_1. These zeros are spreaded due to the wide angular resolution of the detector and become smoothed and angularly shifted minimums in the observed electron distributions. Theoretical values follow this trend when averaged over the experimental resolution.

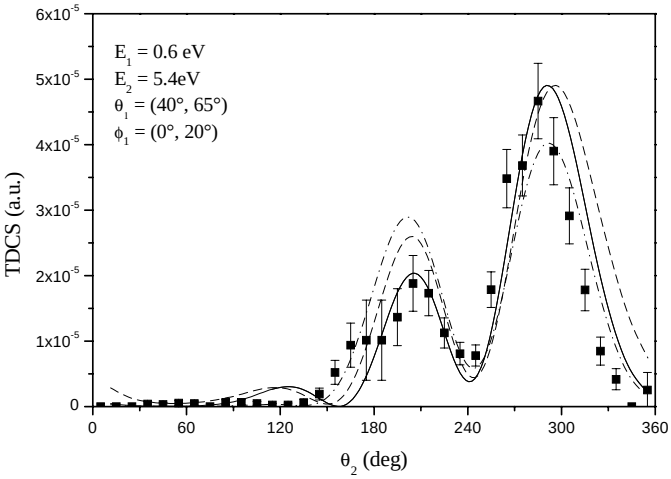

Fig. 1. TDCS as a function of θ_2 for $E_\gamma = 85$ eV and $E_1/E_\mathrm{f} = 0.1$. Theories are given by: solid line: SC3 model in velocity gauge; dot-dashed line: SC3 model in length gauge; dashed line: C3 model in velocity gauge. The scaling factors associated to the theories to reach the data are 5, 0.43 and 227 respectively.

In Figures 1–3 we respectively consider $R = E_1/E_\mathrm{f} = 0.1, 0.5, 0.9$ for $E_\mathrm{f} = 6$ eV. The detection angular range is $\theta_1 = (40°-65°)$ and $\varphi_1 = (0°-20°)$. The present theory in velocity and length gauges is compared with the C3 model in velocity gauge. On sake of simplicity we have not included the results of the C3 model in the length gauge. The relation between the TDCS with the C3 model in both gauges is similar to the relation observed for the SC3 model. In Figure 1, it could be seen that the predictions in the velocity gauge of the SC3 and C3 models clearly differ. This shows that the effect of the present model is not simply a scaling factor, but a different modelling of the zone where the electrons are supposed to be closer.

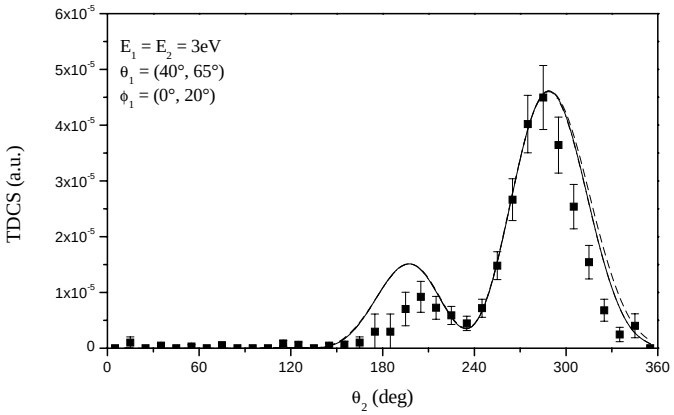

Fig. 2. TDCS as a function of θ_2 for $E_\gamma = 85$ eV and $E_1/E_\mathrm{f} = 0.5$. Theories are as in Figure 1. The corresponding scaling factors are given by 2.3, 0.252 and 96.

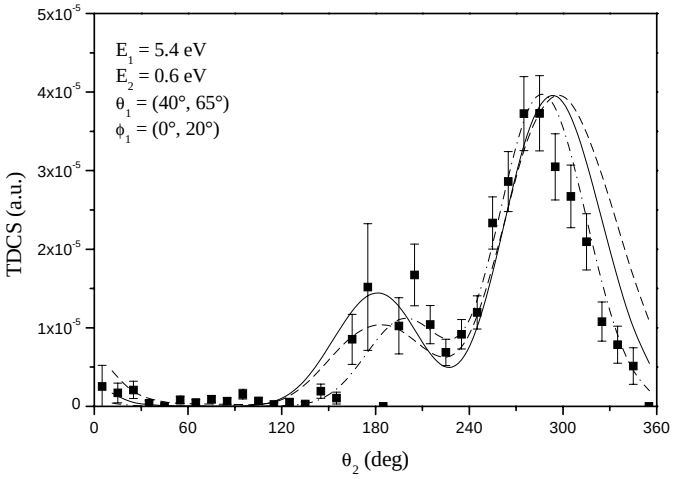

Fig. 3. TDCS as a function of θ_2 for $E_\gamma = 85$ eV and $E_1/E_\mathrm{f} = 0.9$. Theories are as in Figure 1. The corresponding scaling factors are 4.5, 0.405 and 194.

The results in the velocity and length gauges clearly differ in magnitude and so does the ratio between peaks. However, the main features are well given by both forms. In Figure 2 the equal energy regime is shown. It could be seen that besides an scaling factor, the angular predictions in both gauges for the SC3 coincide and could be hardly distinguished one from the other. The results are also in good agreement with the C3 ones. However the scaling factor associated to reach the experiments is much higher for the C3 model. In Figure 3 the slow electron angular distribution is considered. The SC3 in the velocity gauge leads to a better angular distribution than the C3 model but clearly differs with the length gauge.

In Figures 4–6 we respectively consider $R = E_1/E_\mathrm{f} = 0.1, 0.5, 0.9$ for $E_\mathrm{f} = 20$ eV. The detection angular range is $\theta_1 = (20°{-}40°)$ and $\varphi_1 = (0°{-}20°)$. In Figure 4, the fast electron distribution is analyzed. The results of both theories in the velocity gauge agree in shape but the SC3 results are again closer in magnitude to experiment. The length gauge results again predict a different ratio between peaks. In Figure 5 the electrons leave the atom equally

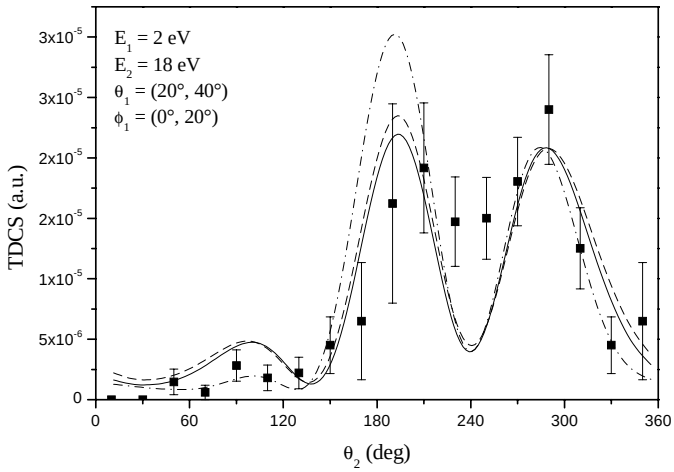

Fig. 4. TDCS as a function of θ_2 for $E_\gamma = 99$ eV and $E_1/E_\mathrm{f} = 0.1$. Theories are as in Figure 1. The corresponding scaling factors associated to the theories are 1.5, 0.195 and 2.75.

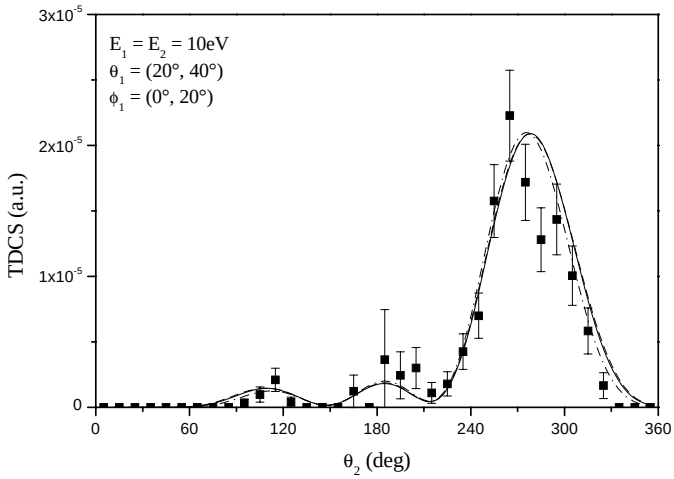

Fig. 5. TDCS as a function of θ_2 for $E_\gamma = 99$ eV and $E_1/E_\mathrm{f} = 0.5$. Theories are as in Figure 1. The scaling factors associated to the theories are 0.9, 0.108 and 1.62 respectively.

sharing the exceeding energy. It could be seen that the angular predictions for both models are in close agreement. The length gauge results, clearly differ in magnitude with the velocity gauge ones. By the other side, they are in good shape agreement. In Figure 6 the slow electron distribution is presented. Again, both models lead to similar angular distributions. It could be seen that the length gauge calculations lead to a narrower peak than the velocity form.

The TDCS evaluated in both gauges give good descriptions of the angular distributions, but clearly differ in magnitude. Lucey *et al.* [15], have shown that for equal energy electrons, the initial state correlation does not play a substantial role in determining the angular distribution. When using initial states of different accuracy small differences are observed in magnitude of the TDCS in the velocity gauge. By the other side, large discrepancies are obtained with the length gauge calculations. The length gauge transition amplitude includes information

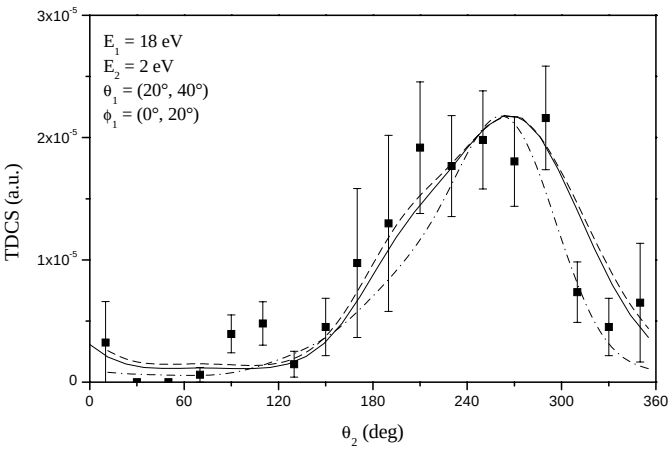

Fig. 6. TDCS as a function of θ_2 for $E_\gamma = 99$ eV and $E_1/E_\mathrm{f} = 0.9$. Theories are as in Figure 1. The scaling factors associated to the theories are 1.5, 0.126 and 2.65 respectively.

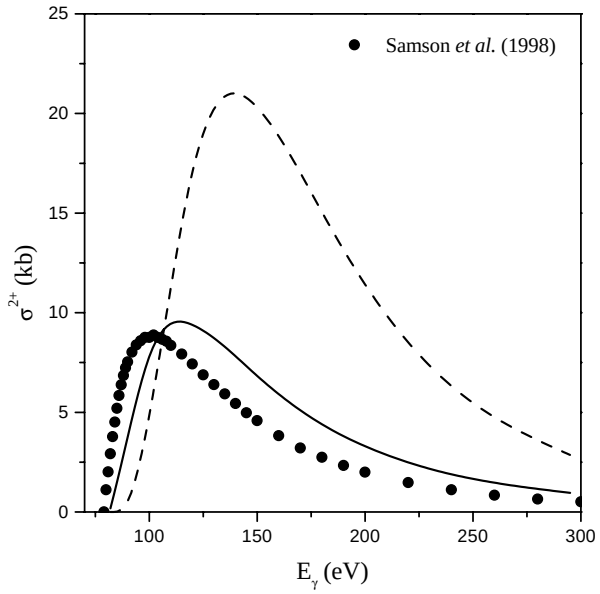

Fig. 7. Total cross-section for PDI of He as a function of the photon energy E_γ. Solid line: SC3; dashed line: C3. Both models are evaluated in velocity gauge.

from larger distances than the velocity gauge one, and enhances the relevance of the initial and final state behavior at long distances.

Functionally simple bound states give with precision the value of the bound energy, but the length TDCS for PDI strongly depends of the spatial distribution of this wave. In a recent work [29], Kheifets and Bray show within the convergent close coupling (CCC) scheme that the initial state correlation does play a leading role in the agreement of the results of the velocity and length gauges. They compare Hartree-Fock-type wave functions against Hylleras-type wave functions in order to accurately represent the He ground state. They find that for Hylleras wave functions the cross-sections in the length gauge converge to the velocity gauge values as the number of parameters considered increases. By the other side, Hartree-Fock wave functions give disagreement between gauges even when a large number of terms are included. In the present model we found the disagreement between the magnitude of the TDCS evaluated in the velocity and length gauges. However this is probably a consequence of the simple initial state used and results could improve with a more sophisticate bound state.

In Figure 7, we show the total cross-section for PDI (σ^{2+}) calculated in the velocity gauge as a function of the photon energy. For comparison we include the experimental data of Samson *et al.* [30]. For $E_\gamma \geq 100$ eV, it could be seen that the C3 model largely overestimates the experimental data in the intermediate energy zone. Meanwhile the SC3 model leads to a good agreement with data in shape and magnitude. The simple $\beta(E_\mathrm{f})$ proposed in equation (6), represents an improvement of the standard C3 model but it is not enough to compensate the exponential decreasing behavior of the TDCS in the limit $E_\mathrm{f} \to 0$. It is well known that the total cross-section for PDI in this limit is given by,

$$\sigma^{++} = \sigma_0 E_\mathrm{f}^{\alpha} \tag{9}$$

where $\alpha = 1.056$ is the Wannier exponent and σ_0 is the value of σ^{++} at $E_\mathrm{f} = 1$ eV. Kossmann *et al.* [31], have performed an extensive study of the threshold law equation (9). They have fit their experimental data with equation (9) obtaining the values of $\sigma_0 = 1.02 \times 10^{-21}$ cm^2 and $\alpha = 1.05$. They also found this threshold law meaningless for exceeding energies above 2 eV. A further correction of the SC3 model is required in the Wannier region. We have assumed a very simple energy dependence for the β parameter and a good strategy to correct the Wannier region could be given by expressing,

$$\beta = \frac{f(E_\mathrm{f})}{\sqrt{E_\mathrm{f}}}$$

where $f(E_\mathrm{f})$ must be a function which goes to 1 as $E_\mathrm{f} \to \infty$. Therefore it could accept an expansion:

$$f(E_\mathrm{f}) = 1 + \frac{a_1}{E_\mathrm{f}} + \frac{a_2}{E_\mathrm{f}^2} + ...$$

The a_j parameters could be fit according to the results of Kossmann *et al.* This correction to equation (6) would then be appreciated in the low energy zone of the spectra of Figure 7. This would be explored in detail in a forthcoming work.

4 Conclusions

The C3 wave describes the $e-e$ motion as independent of the presence of the nucleus, and represents it by a Coulomb continuum wave. The corresponding normalization factor falls exponentially with decreasing relative momentum between the electrons, producing a TDCS that violates the Wannier limit. In this paper we have introduced a multiplicative parameter β in the interelectronic coordinate that tights the $e-e$ wave at short distances,

indirectly accounting for the screening effect of the nuclear ion. This increases the superposition between the final and initial state in the transition amplitude, and can be chosen to compensate the exponential decrease of the normalization.

The parameter β depends on the total energy of the emerging electrons. We have proposed a functional form that for large energies leads to an uncorrelated model, and tends to correct the C3's usual magnitude failure for low and intermediate exceeding energies. The effects the present modification introduces in the continuum wave function, could be also seen in the Ω_0 region, where a phase factor resumes the accumulated phase that could be attached to the nuclear presence.

We have calculated TDCSs for photon impact on He, in the dipole approximation in the velocity and length gauges. We found very good agreement in angular shape with available experimental data and a clear enhancement of the magnitude of the TDCS in the range 6–20 eV of exceeding energy.

We have shown that the present model improves the theoretical total cross-section for photon energies greater than about 100 eV in contrast with the C3 model where correct values are reached for energies greater than 1 keV.

We would like to thank G. Gasaneo, W.R. Cravero and M.F. Ciappina for fruitful discussions, and Dr. R. Dörner for communicating their tabulated data. This work has been supported by CONICET and PICT 99/03/06249 and 98/03/04021 of the APCYT (Argentina).

References

1. A. Dalgarno, R.W. Ewart, Proc. Phys. Soc. **80**, 616 (1962)
2. J.S. Briggs, V. Schmidt, J. Phys. B: At. Mol. Opt. Phys. **33**, R1 (2000)
3. G. King, L. Avaldi, J. Phys. B: At. Mol. Opt. Phys. **33**, R215 (2000)
4. F.W. Byron, C.J. Joachain, Phys. Rev. **164**, 1 (1967)
5. M. Pont, R. Shakeshaft, Phys. Rev. A **51**, R2676 (1995)
6. D. Proulx, R. Shakeshaft, Phys. Rev. A **48**, R875 (1993)
7. M.R.H. Rudge, M.J. Seaton, Proc. R. Soc. A **283**, 262 (1965)
8. M. Pont, R. Shakeshaft, F. Maulbescht, J.S. Briggs, Phys. Rev. A **53**, 3671 (1996)
9. C.R. Garibotti, J.E. Miraglia, Phys. Rev. A **21**, 572 (1980)
10. M. Brauner, J.S. Briggs, H. Klar, J. Phys. B: At. Mol. Opt. Phys. **22**, 2265 (1989)
11. F. Maulbescht, J.S. Briggs, J. Phys. B: At. Mol. Opt. Phys. **26**, L647 (1993); J. Phys. B: At. Mol. Opt. Phys. **27**, 4095 (1994)
12. G. Gasaneo, F.D. Colavecchia, C.R. Garibotti, J.E. Miraglia, P.A. Macri, Phys. Rev. A **55**, 2809 (1997)
13. J. Berakdar, J.S. Briggs, Phys. Rev. Lett. **72**, 3799 (1994)
14. J. Berakdar, Phys. Rev. A **53**, 2314 (1996)
15. S.P. Lucey, J. Rasch, C.T. Whelan, H.R.J. Walters, J. Phys. B: At. Mol. Opt. Phys. **31**, 1237 (1998)
16. M.A. Kornberg, V.D. Rodriguez, Eur. Phys. J. D **5**, 221 (1999)
17. A.S. Kheifets, I. Bray, Phys. Rev. A **54**, R995 (1996); J. Phys. B: At. Mol. Opt. Phys. **31**, L447 (1996); Phys. Rev. A **57**, 2590 (1998)
18. J. Colgan, M.S. Pindzola, F. Robicheaux, J. Phys. B: At. Mol. Opt. Phys. **34**, L457 (2001)
19. L. Malegat, P. Selles, A.K. Kazansky, Phys. Rev. Lett. **85**, 4450 (2000)
20. J.E. Miraglia, M.G. Bustamante, P.A. Macri, Phys. Rev. A **60**, 4532 (1999)
21. S.J. Ward, J.H. Macek, Phys. Rev. A **49**, 1049 (1994)
22. M. Brauner, J.S. Briggs, H. Klar, J.T. Broad, T. Rösel, K. Jun, H. Ehrhardt, J. Phys. B: At. Mol. Opt. Phys. **24**, 657 (1991)
23. R.A. Bonham, D.A. Kohl, J. Chem. Phys. **45**, 2471 (1966)
24. M. Kornberg, J.E. Miraglia, Phys. Rev. A **48**, 3714 (1993); Phys. Rev. A **49**, 5120 (1994)
25. F. Maulbetsch, M. Pont, J.S. Briggs, R. Shakeshaft, J. Phys. B: At. Mol. Opt. Phys. **28**, L341 (1994)
26. R. Dörner, H. Bräuning, J.M. Feagin, V. Mergel, O. Jagutzki, L. Spielberger, T. Vogt, H. Khemliche, M.H. Prior, J. Ullrich, C.L. Cocke, H. Schmidt-Böcking, Phys. Rev. A **57**, 1074 (1998)
27. J. Ullrich, R. Moshammer, O. Jagutzki, V. Mergel, L. Spielberger, J. Phys. B: At. Mol. Opt. Phys. **30**, 2917 (1997)
28. F. Maulbetsch, J.S. Briggs, J. Phys. B: At. Mol. Opt. Phys. **28**, 551 (1995)
29. A.S. Kheifets, I. Bray, Phys. Rev. A **57**, 2590 (1998)
30. J.A.R. Samson, W.C. Stolte, Z.-X. He, J.N. Cutler, Y. Lu, R.J. Bartlett, Phys. Rev. A **57**, 1906 (1998)
31. H. Kossmann, V. Schmidt, T. Andersen, Phys. Rev. Lett. **60**, 1266 (1988)